



# Radiation damage in the TEM and SEM

R.F. Egerton\*, P. Li, M. Malac

*Department of Physics, University of Alberta, Faculty of Science, 412 Avadh Bhatia Phy, Edmonton T6G 2J1, Canada*

## Abstract

We review the various ways in which an electron beam can adversely affect an organic or inorganic sample during examination in an electron microscope. The effects considered are: heating, electrostatic charging, ionization damage (radiolysis), displacement damage, sputtering and hydrocarbon contamination. In each case, strategies to minimise the damage are identified. In the light of recent experimental evidence, we re-examine two common assumptions: that the amount of radiation damage is proportional to the electron dose and is independent of beam diameter; and that the extent of the damage is proportional to the amount of energy deposited in the specimen.

© 2004 Elsevier Ltd. All rights reserved.

*Keywords:* Radiation damage; Radiolysis; Electron sputtering; Transmission electron microscope; Scanning electron microscope

## 1. Introduction

Besides providing useful information, the electron beam used in a transmission electron microscope (TEM) or scanning electron microscope (SEM) can cause temporary or permanent change in the surface or bulk structure of a specimen. One way of categorizing this damage is in terms of the type of electron scattering that gives rise to it (Fig. 1).

*Elastic* scattering represents electrostatic deflection of incoming electrons by the Coulomb field of each atomic nucleus. It gives rise to electron-diffraction patterns and to diffraction and phase contrast in TEM images, as well as backscattered-electron (BSE) contrast in SEM images, but in some circumstances can result in atomic displacement within a crystalline specimen or electron-beam sputtering of atoms from its surface.

*Inelastic* scattering represents Coulomb interaction of incoming electrons with the atomic electrons that surround each nucleus. It gives rise to the secondary-electron production that provides SEM images, to the emission of X-rays (used for elemental analysis in the SEM and TEM) and to electron energy-loss spectra (EELS) in the TEM. But inelastic scattering can also produce radiolysis effects, which change the structure of a specimen or remove material (mass loss). Under certain conditions (the presence of ambient hydrocarbons), electronic excitation also causes

hydrocarbon contamination, which obscures or distorts the TEM or SEM image.

The first part of this paper consists of a brief review of our current knowledge about these various damage processes, including steps that may be taken to avoid or minimize them. In the second part, we examine some recent experimental results that challenge two common assumptions in the field of radiation research: that the damage is proportional to the accumulated radiation dose, and is proportional to the amount of deposited energy. In order to resolve these issues, further experiments are suggested.

## 2. Atomic displacement

It is convenient to assume that elastic scattering involves no change in energy of the transmitted beam. However, conservation of energy and momentum dictates that an electron which is deflected through an angle  $\theta$  in the field of a single atomic nucleus (atomic mass number  $A$ ) must transfer an amount of energy  $E$  given (in eV) by:

$$E = E_{\max} \sin^2(\theta/2) \quad (1)$$

$$E_{\max} = E_0(1.02 + E_0/10^6)/(465.7A) \quad (2)$$

where the incident-electron energy  $E_0$  is also in eV. For small angles of scattering, as recorded in a typical TEM diffraction pattern, the  $\sin^2$  term in Eq. (1) ensures that

\* Corresponding author. Tel.: +1-780-482-5095; fax: +1-780-492-0714.  
E-mail address: [regerton@ualberta.ca](mailto:regerton@ualberta.ca) (R.F. Egerton).

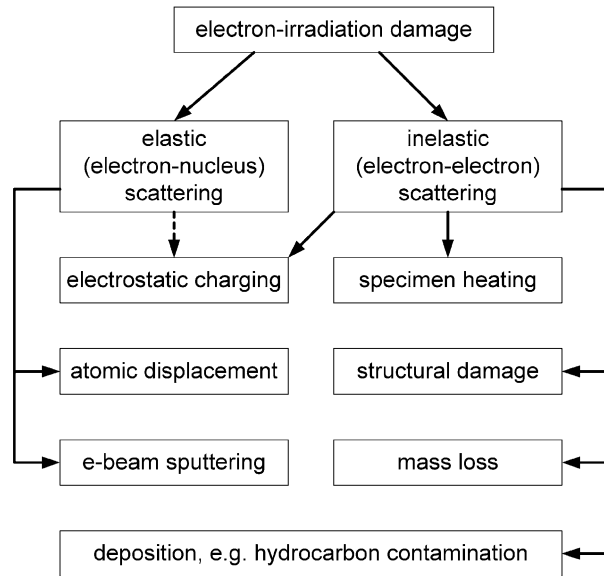


Fig. 1. Classification of radiation damage according to the type of electron scattering and according to the effects produced in a specimen.

the energy transfer is negligible ( $\ll 1$  eV) but for backscattering ( $\theta > 90^\circ$ ) and high  $E_0$ , the energy loss  $E$  may be several eV. For a head-on ‘collision’ with the nucleus,  $\theta = 180^\circ$  and Eq. (1) gives  $E = E_{\max}$  which may be many eV for high  $E_0$  and atoms of low atomic weight (mass number)  $A$ , as can be deduced from Eq. (2).

If  $E$  exceeds some *displacement energy*  $E_d$  which is a property of the specimen material (bond strength, crystal lattice and atomic weight of the constituent atoms), high-angle elastic scattering can displace atomic nuclei to interstitial positions and thereby degrade the crystalline perfection. This effect is most easily seen in the TEM if the specimen is raised to an elevated temperature, such that the interstitials aggregate to form loops or defect clusters which give a characteristic ‘black-white’ diffraction contrast (Fig. 2). Similar effects are seen in metals that have

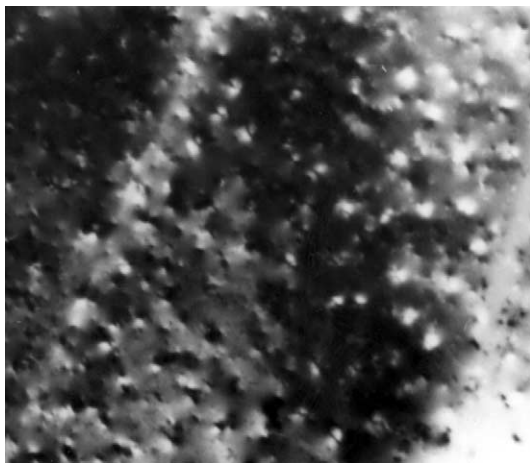


Fig. 2.  $2 \mu\text{m} \times 2 \mu\text{m}$  bright-field TEM image showing defect clusters produced in a thin graphite crystal irradiated at  $600^\circ\text{C}$  by 200 keV electrons.

Table 1

Displacement energy  $E_d$ ; and the corresponding threshold value of incident energy  $E_0$ , for some common materials (Hobbs, 1987)

Material	$E_d$ (eV)	$E_0$ (keV)
Graphite	30	140
Diamond	80	330
Aluminum	17	180
Copper	20	420
Gold	34	1320

been exposed at elevated temperature to neutron or ion bombardment.

Some experimentally-determined values of  $E_d$  are given in Table 1, together with the corresponding threshold energy (value of  $E_0$  above which displacement occurs) obtained by setting  $E_{\max} = E_d$  in Eq. (2). The accelerating voltages used in an SEM are too low to induce displacement damage. In the TEM, displacement effects are not expected for  $E_0 = 100$  keV (unless the specimen contains hydrogen atoms) but the specimen is vulnerable at higher energies, especially if it contains atoms of low or medium atomic number. For example, carbon nanotubes or crystalline silicon can be safely imaged in the TEM at 100 kV but not at 200 kV accelerating voltage.

Since it does not affect the momentum transfer to a nucleus, specimen temperature cannot be used as a means of controlling the displacement process. The only sure way of avoiding displacement damage is to use an incident energy below the threshold energy for the material in question. If higher energies must be used, the electron dose (product of current density and recording time) should be limited to the minimum that is sufficient to record the information required.

### 3. Electron-beam sputtering

If high-angle elastic scattering occurs at an atom (atomic number  $Z$ , mass number  $A$ ) which lies at the *surface* of a specimen, Eqs. (1) and (2) remain valid but the energy  $E_s$  required for displacement is much lower: surface atoms do not have to be squeezed into an interstitial site—they are free to leave the specimen and enter the vacuum of the microscope. By analogy with the displacement of surface atoms by *ion* beams, this process is called *sputtering*. The removal of carbon (from small carbide precipitates by a focused field-emission probe) has been attributed to this process, largely on account of the relatively small temperature dependence observed (Thomas, 1985).

It is believed that a sputtering crater forms only on the beam-exit surface, since the momentum transfer involved in a high-angle collision is mainly in the incident direction (Crozier et al., 1990; Medlin and Howitt, 1991). Sputtering

problems are therefore unlikely in the SEM, especially since the incident energy and current density are lower than in the TEM.

Analogous to the case of atomic displacement within a specimen, electron-beam sputtering occurs only for an incident energy  $E_0$  which exceeds some *threshold* value, given by  $E_{\max} = E_s$ . Taking  $E_s$  as the sublimation energy per atom, threshold energies for some common elements, estimated using Eq. (2), are shown in Fig. 3. Light and medium-Z atoms appear to be vulnerable to sputtering by 200 keV electrons.

The sputtering rate  $S$  (in monolayers per second) is given approximately by:

$$S = (J/e)(Z^2/AE_0)(1/E_s - 1/E_{\max})(3.54 \times 10^{-17} \text{ cm}^2) \quad (3)$$

in which  $(J/e)$  represents the incident-current density in *electrons/cm<sup>2</sup>/s* and the remainder of the expression is a sputtering cross-section, here evaluated using a non-relativistic Rutherford-scattering model;  $E_s$  is in eV and  $E_{\max}$  is related to the incident energy through Eq. (2). The case of elemental carbon, shown in Fig. 4, illustrates the fact that the sputtering rate increases rapidly above the incident-energy threshold, comes close to its maximum value at about *twice* the threshold value and varies relatively little at higher incident energy. Because the sputtering rate is low *immediately above* the incident-energy threshold, the situation for medium-Z elements is somewhat less serious than might be deduced by immediate inspection of Fig. 3.

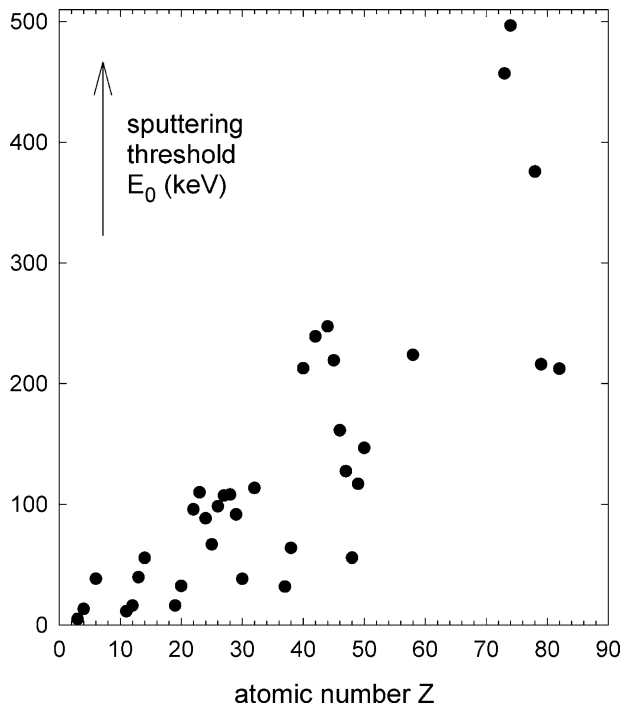


Fig. 3. Threshold incident energy for onset of electron sputtering in solid elements, calculated using Eq. (2) taking  $E_s$  as the sublimation energy per atom.

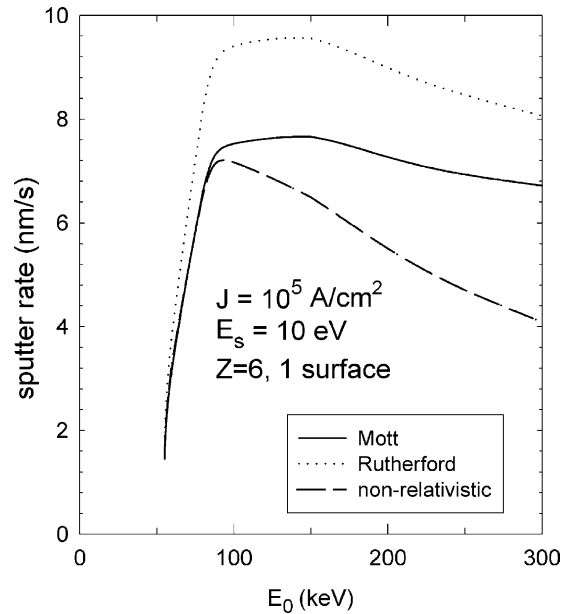


Fig. 4. Sputtering rate (in nm/s) at the exit surface of a carbon film versus incident-electron energy  $E_0$ , based on relativistic Mott and Rutherford and Mott cross-sections, and as given by Eq. (3).

In crystalline specimens, focused collision sequences can transfer momentum over a short distance (a few atomic layers) to surface atoms, thereby increasing the sputtering rate (Cherns et al., 1976). However, this effect is important only for incident energies well above the threshold energy (Cherns et al., 1977). Therefore a layer of high-Z material (e.g. tungsten, threshold  $\approx 500$  keV) on the *exit* surface of a TEM specimen could protect against mass loss in high-intensity beams.

The sputtering rates calculated in Fig. 4 are for an incident-current density of  $J = 10^5$  A/cm<sup>2</sup>, just achievable using a 200 keV field-emission TEM with focused illumination and a large condenser aperture. Holes in a 20 nm carbon film are formed in a few seconds under such conditions. In the case of a field-emission TEM fitted with an aberration-corrected probe-forming lens, the current density can exceed  $10^6$  A/cm<sup>2</sup> (Lupini et al., 2001) and sputtering effects should be readily observable with a stationary probe and non-contaminating conditions.

As illustrated in Fig. 3, sputtering mainly involves low-Z atoms (even if these are contained in a high-Z matrix). If the threshold incident energy is low, the best strategy for avoiding sputtering is to limit the radiation dose. Where this is not possible (e.g. elemental analysis by energy-loss or x-ray spectroscopy), a thin layer of a heavy element which completely covers the beam-exit surface may provide protection for TEM specimens.

#### 4. Electron-beam heating

Because *inelastic* scattering involves ‘collision’ between the incoming electrons and particles (atomic electrons) of

similar mass, appreciable energy can be transferred in the process. Most of this energy ends up as heat within the specimen, giving rise to a local temperature  $T$  that is higher than the temperature  $T_0$  of the surroundings.

Consider first the case of a thin specimen (thickness  $t$ ) in the TEM. If the average energy loss *per inelastic collision* is  $\langle E \rangle$ , the average energy *per incident electron* is  $\langle E \rangle (t/\lambda)$  where  $\lambda$  a mean free path for all inelastic scattering. The heat deposited in the specimen per second is therefore  $(I/e)\langle E \rangle (t/\lambda)$ ;  $I$  is the beam current and  $e$  the electronic charge. This expression can be rewritten as  $I\langle E(\text{eV}) \rangle (t/\lambda)$  where the average energy is now expressed in eV rather than Joule. A steady state is quickly achieved in which the heat generation (in an incident beam of diameter  $d$ ) is balanced by heat loss due to radial conduction (over a distance  $R_0$  through material of thermal conductivity  $\kappa$ ) and radiation (from both surface of the specimen, emissivity  $\varepsilon$ ):

$$I\langle E(\text{eV}) \rangle (t/\lambda) = 4\pi\kappa t(T - T_0)/[0.58 + 2\ln(2R_0/d)] + \pi(d^2/2)\varepsilon\sigma(T^4 - T_0^4) \quad (4)$$

Putting numbers into Eq. (4) shows that the radiation term can generally be neglected, even for relatively poor thermal conductors. As a result, the temperature rise ( $\Delta T = T - T_0$ ) becomes *independent* of specimen thickness.

Beam heating is known to be a problem in the TEM at high incident currents, for example if a large (or no) condenser-lens aperture is used. Under such conditions, thin specimens of common metals have been melted in a tungsten-filament TEM, despite their relative good thermal conductivity ( $\kappa > 100\text{W/m/K}$ ). But even at low current densities, heating effects are worrisome for organic materials such as polymers, where  $\kappa$  can be quite low (0.2–2 W/m/K) and the materials are susceptible to melting or thermal degradation at only moderately elevated temperatures.

Although electron probes of very small diameter may involve a high current density, the temperature rise is usually insignificant. Applying Eq. (4) to a 5 nA stationary probe incident on a carbon film ( $\kappa \approx 1.6\text{W/m/K}$ ) gives the results shown in Fig. 5; as the beam diameter is decreased from 1  $\mu\text{m}$  to 1 nm, the current density in the probe increases by a factor of  $10^6$  but  $\Delta T$  increases only from 0.5 to 1.4 K. This small increase is a result of the logarithmic term in Eq. (4), which is a characteristic of two-dimensional radial heat flow. Consequently, the temperature rise involved in scanning-transmission (STEM) imaging would not be much greater from that involved in TEM imaging, *even if* the incident-beam current were the same.

In the case of SEM, a *bulk* specimen is normally used and heat flow is radial in *three* dimensions, leading to a relatively small temperature rise. When the probe diameter is much less than the electron range  $R$ , the temperature rise in a stationary probe is (Reimer, 1998, p. 118):

$$\Delta T = (1.5/\pi)(IV_0)/(\kappa R) \quad (5)$$

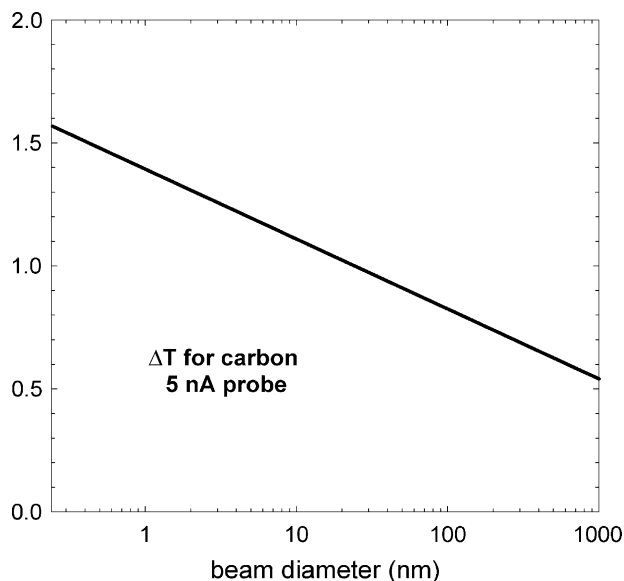


Fig. 5. Temperature rise ( $\Delta T$ ) in a carbon film for a 5 nA electron probe, calculated as a function of the probe diameter ( $d$ ) using Eq. (4) with  $R_0 = 30 \mu\text{m}$  and  $\kappa = 1.6 \text{W/m/K}$ . Incident energy = 200 keV.

where  $I$  is the probe current and  $V_0$  the accelerating voltage. For  $V_0 = 20 \text{kV}$  and  $I = 1 \text{nA}$ ,  $R \approx 1 \mu\text{m}$  and  $\Delta T < 0.1 \text{K}$  for metals or a few degrees for a typical polymer ( $\kappa \approx 1 \text{W/m/K}$ ). With a *scanning* probe, whose dwell time per pixel is typically less than the thermal equilibration time,  $\Delta T$  is even lower.

But if a thin film (on a TEM grid) is examined in the SEM and if the incident energy is between 500 eV and 2 keV, the temperature rise in an organic specimen can reach a few hundred degrees for a stationary probe (Li, 2003). In this situation, the electron range is less than the film thickness, all of the beam energy is deposited in the film and the heat flow is two-dimensional. The temperature rise is typically reduced by a factor of ten if the beam is scanned at video rate.

## 5. Electrostatic charging

The charging of electrically-insulating specimens involves both elastic and inelastic scattering, since the net charge added to the film per second depends both on the backscattering coefficient  $\eta$  and on the yield  $\delta(\varepsilon)$  for secondary electrons which are emitted with kinetic energy  $\varepsilon$ . Consider first the case of a bulk SEM specimen; analogous to Eq. (4), the steady-state condition represents a current balance:

$$I + V_s/R_s = I\eta + I\delta(V_s) = I\eta + I \int (d\delta/d\varepsilon)d\varepsilon \quad (6)$$

where  $V_s$  is the surface potential developed in the beam and  $R_s$  is an effective electrical resistance between the irradiated and surrounding regions of specimen. Terms on the left-hand side of Eq. (6) represent *negative* current entering

the irradiated volume, from the beam (incident current  $I$ ) and by leakage (from a grounded specimen stage) through the specimen. Terms on the right-hand side represent the loss of electrons by backscattering and by secondary emission;  $\delta(V_s)$  is an effective secondary yield when the surface potential is  $+V_s$ , such that electrons of energy below  $eV_s$  cannot escape into the vacuum. Appropriate limits of the integral in Eq. (6) are therefore  $eV_s$  and (approximately)  $E_0 - eV_s$ , this last expression representing the kinetic energy of the highest-energy secondary which can be generated by incident electrons of energy  $E_0$ .

At high  $E_0$ , most secondary electrons are generated well below the surface of the specimen and do not escape into the vacuum. Consequently,  $\delta(V_s)$  is low and a negative value of  $V_s$  is needed, on the left-hand side of Eq. (6), to achieve current balance, as seen in Fig. 6. If  $R_s$  is large (highly insulating specimens),  $|V_s|$  may be many kV, causing the incident beam to be repelled from the charged region and giving rise to unstable or distorted SEM images (Reimer, 1998).

At low  $E_0$ , the beam penetrates only a few nm (or less) and most of the secondaries produced can escape. The larger value of  $\delta(V_s)$  requires  $V_s$  to be positive in order to achieve current balance. After the beam hits the specimen, the rise in  $V_s$  causes  $V_s/R_s$  to increase and  $\delta(V_s)$  to decrease until Eq. (6) is satisfied. For highly insulating materials (large  $R_s$ ), the

$V_s/R_s$  term is insignificant but balance can still be achieved, at a surface potential  $V_s$  which is sufficient to prevent the lower-energy secondaries from leaving. Nevertheless, it is advantageous to work at a particular incident energy  $E_0 = E_2$  (Fig. 6) at which the required value of  $V_s$  is zero, since this avoids loss of secondary-electron signal. Values of  $E_2$  have been tabulated for common materials (Joy and Joy, 1996).

At very low incident energy ( $E_0 < E_1$ ), primary electrons have insufficient energy to generate many secondaries. Because  $\delta$  is low and since  $\eta < 1$ ,  $V_s$  again becomes negative. However, values of  $E_1$  are typically in the range 50–150 eV (Joy and Joy, 1996) and therefore not relevant to most scanning-electron microscopy.

In the case of a thin specimen in the TEM, current balance requires that a term representing the transmitted electron current  $I_t$  be added to Eq. (6), giving:

$$I - I_t + V_s/R_s = I\eta(t) + I\delta(V_s) \quad (7)$$

Here  $\eta(t)$  is a reduced backscattering coefficient, taking into account the small thickness  $t$  of the specimen. As  $t$  is reduced,  $I_t$  approaches  $I$  in magnitude since very few electrons are absorbed within a thin specimen, especially at high  $E_0$ . The effect of increasing  $I_t$  is to cause  $V_s$  to again become positive above some incident energy  $E_3$ , typically 2–10 keV (Reimer et al., 1992; see dashed curves in Fig. 6). Under these positive-charging conditions, the surface potential  $V_s$  can increase so that current balance is achieved, as for a bulk specimen with  $E_1 < E_0 < E_2$ . Statistical fluctuations in  $V_s$  may account for the fluctuating granularity (bee-swarm effect) sometimes seen in the TEM image of a thin insulating film (Curtis and Ferrier, 1969).

At high current density, and taking into account the existence of Auger electrons with high kinetic energy,  $V_s$  may become dangerously high, as pointed out by Cazaux (1995) who analysed the case of a typical field-emission probe ( $d = 1$  nm,  $I = 0.4$  nA) and obtained  $V_s = 76$  eV. While this voltage may have negligible effect on the electron focusing, it leads to an electric field (at the edges of the illuminated area) in excess of  $10^{10}$  V/m, sufficient to cause electrical breakdown (Hobbs, 1990) and possibly a lateral migration of ions. Calculation of the corresponding net charge within the irradiated volume (containing  $n$  atoms) gave  $Q_s \approx 1000e \approx 0.16n$  (Cazaux, 1995). Since a solid with 16% of its atoms ionized is likely to disintegrate by electrostatic repulsion, electrostatic charging was proposed as an explanation of the hole drilling observed in metal-oxide insulators in a field-emission STEM (Humphreys et al., 1990).

Charging of a TEM specimen can also produce a mechanical force that the specimen is unable to withstand. For example, it may cause tearing of thin polymer films, especially since mechanical softening (due to the heating effect of the beam) is likely.

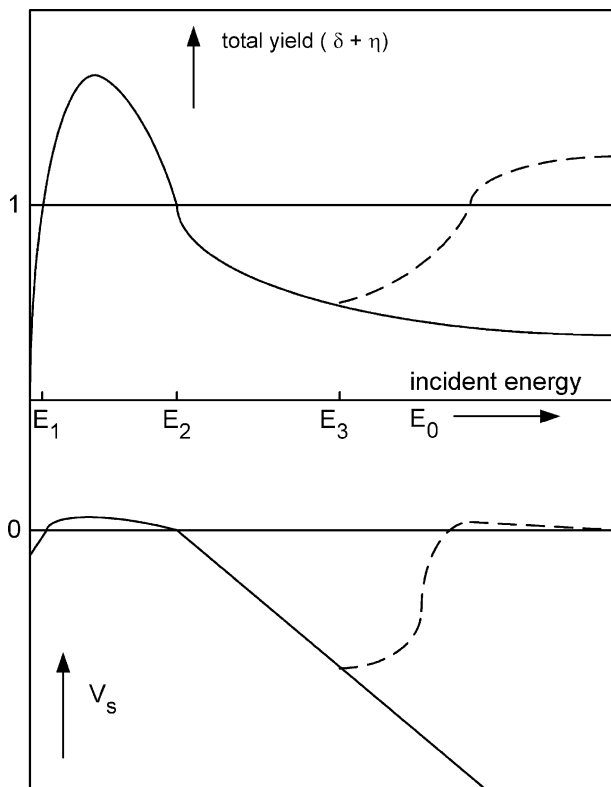


Fig. 6. Total electron yield ( $\delta + \eta$ ) and surface potential ( $V_s$ ) in a poorly conducting bulk specimen or thin film (dashed curve), as a function of incident-beam energy  $E_0$ .

## 6. Radiolysis of inorganic materials

Radiolysis implies electron-beam degradation through *inelastic* scattering. To produce atomic displacement (loss of crystallinity or mass loss), there must be some mechanism for converting the energy acquired by atomic electrons to kinetic energy and momentum of atomic nuclei. For alkali halides, which are among the most radiation-sensitive inorganic materials, inelastic scattering can lead to a 7 eV exciton state, which decays within 10 ps to form an double-halogen ion (H-centre) and an anion vacancy (F-centre), as described by Hobbs (1984). The vacancies can aggregate to form voids and the displaced halogen ions may condense to create dislocation loops but will eventually diffuse to the surface, resulting in halogen loss (Egerton et al., 1987). Radiolysis is somewhat temperature dependent and can be reduced by cooling the sample (Hobbs, 1984, 1990).

Other binary compounds such as oxides decompose in an electron beam, but at much higher doses and in the case of a highly focussed probe the mechanism may involve electrostatic charging, as discussed above. Whereas elastic displacement occurs only above some incident electron energy, hole drilling seems to occur only above some threshold *current* density, easily achieved in field emission probes (Salisbury et al., 1984; Humphreys et al., 1990) and less easily with a thermionic source (Devenish et al., 1989). If so, the problem may be worse for STEM imaging than for TEM with the same accumulated dose.

In the case of transition-metal oxides, radiolysis is believed to occur via the Knotek-Feibelman mechanism: the incident electron creates an inner-shell vacancy on the metal site followed by (interatomic) Auger decay from the oxygen. This results in a (neutral or) positive O atom which is repelled by the surrounding metal ions and ejected into the vacuum leaving a metal-rich surface with a mottled (pitted) appearance (McCartney et al., 1991). The process continues until the material becomes sufficiently conducting to screen the positive oxygen ion. Since the mass loss occurs mainly close to the surface of the specimen, it is also known as electron-stimulated desorption (ESD).

For inorganic specimens, the existence of a radiolytic process increases the thinning rate above that due to electron-beam sputtering and may pose a severe problem in the case of a stationary aberration-corrected probe. Conversely, an aberration-corrected instrument could be very useful for electron-beam lithography on a sub-nm scale (Broers, 1988; Humphreys et al., 1990)

## 7. Radiolysis of organic materials

The worst problems of radiation damage occur in *organic* solids, which are either amorphous (e.g. most polymers) or molecular crystals, containing both covalent bonds and much weaker (Van der Waals) bonding. Electron

excitation occurs *within* each molecule but (partly due to the weak steric constraints) the subsequent de-excitation may not return the molecule to its original electronic state. In other words, chemical bonds are broken and the molecule changes in shape and shifts in position, causing a loss of crystallinity which is observed as a fading of the spots in an electron-diffraction pattern (Henderson and Glaeser, 1985). The change in electronic configuration of a molecule also causes a loss of fine structure in the electron energy-loss spectrum, while the bond breakage results in mass loss (escape of light atoms: particularly hydrogen, nitrogen and oxygen).

For each of these processes, a *critical dose* can be defined, for example for ‘complete’ destruction of the electron-diffraction pattern of a crystalline sample. Note that in the electron-microscope literature, ‘dose’ usually means *electron exposure* (often in C/cm<sup>2</sup>), the product of incident-current density and exposure time. As shown in Table 2, this critical dose varies widely between different organic materials but is generally higher for aromatic compounds compared to aliphatic ones. The higher radiation stability of the aromatics is attributed to the fact that they contain relatively stable ring structures, with a high resonance energy of the  $\pi$ -electrons (Isaacson, 1975) which allows the energy deposited by inelastic scattering to be shared by many electrons without bond breakage.

As noted by Isaacson (1977), the dose required for mass loss and composition change in an organic material is usually greater than the dose which gives diffraction-pattern fading (loss of long-range order) but less than that required for loss of energy-loss fine structure (destruction of short-range molecular order). In molecular crystals, the size of each molecule is not much smaller than that of the unit cell, so a distortion of the molecular shape (due to limited bond breakage, possibly accompanied by hydrogen loss) can appreciably affect the diffraction intensities. More extensive irradiation leads to loss of other elements but the stable ring structure of aromatics, as measured by the EELS fine structure (usually the 6 eV  $\pi$ -resonance peak) remains intact.

The release of H atoms is an important factor in the radiation damage process, as illustrated by the reduced sensitivity of phthalocyanine (Pc) in which peripheral H

Table 2  
: Critical dose  $D_c$ ; for destruction of the electron-diffraction pattern of selected aliphatic and aromatic materials (Reimer, 1975)

Material	$E_0$ (keV)	$D_c$ (C/cm <sup>2</sup> )
Glycine	60	0.0015
C <sub>26</sub> paraffin	60	0.004
Polyethylene	100	0.01
Anthracene	60	0.07
Phthalocyanine (Pc)	60	0.1
Cu-phthalocyanine (Cu-Pc)	60	1.5
Cl <sub>16</sub> Cu-phthalocyanine	100	30

atoms have been replaced by halogen (Br or Cl; see Table 2). Surrounding molecules are thought to provide a ‘cage effect’ which hinders the displacement of the larger halogen atoms. Consistent with this idea, damage to chlorinated Pc was found to occur heterogeneously, producing amorphous-like regions within the crystalline matrix (Clark et al., 1980).

A more quantitative measure of damage is a *characteristic* dose  $D_e$ , defined as the dose at which the effect being measured decreases to  $1/e = 37\%$  of its value at the start of irradiation. Whereas  $D_e$  is a measure of the radiation *resistance* of a material, the radiation *sensitivity* can be expressed as a damage cross-section:

$$\sigma_d = e/D_e \quad (8)$$

where  $e$  is the electronic charge. Eq. (8) can give rise to confusion because  $D_e$  (and therefore  $\sigma_d$ ) is a *macroscopic* quantity derived from experiment, whereas a scattering or electron-excitation cross-section is a microscopic quantity expressed as a target area per atom or (alternatively) per molecule. However, if  $\sigma_d$  is found to match some excitation cross-section *per molecule*, this suggests (although it does not prove) that *one* such excitation *per molecule* is responsible for the damage.

It is reasonable to expect a damage cross-section to scale with incident energy  $E_0$  in the same way as the cross-sections for inelastic scattering, i.e. inversely proportional to the square of the electron speed or (approximately) as  $1/E_0$  for  $E_0$  greater than a few keV (Isaacson, 1977). This might suggest that radiolysis can be reduced by using high incident energy; but since the elastic cross-sections are also proportional to  $1/E_0$ , the ratio of damage to (image or spectroscopic) signal remains unaltered.

With a bulk SEM specimen, damage is produced only close to the surface, within the electron range. As  $E_0$  is reduced, this range becomes very small and the surface damage (energy deposition per unit volume) actually increases. But artifacts such as shrinkage of the specimen depend on the depth as well as energy density, so the observed damage effects tend to be less at low incident energy (Joy and Joy, 1996).

Although lowering the temperature of a specimen does not change the inelastic cross-section, it does reduce the sensitivity of an organic specimen to structural damage and mass loss. The reduction factor depends considerably on the material and on the experimental technique, and has been the subject of much debate (International Experimental Study Group, 1986). Cooling a TEM specimen with liquid nitrogen (below 100 K) decreases mass loss by factors between 3 and 100 (Table 3) and can be explained in terms of the reduced atomic mobility at low temperature. In fact, the sample does lose mass when returned to room temperature (without further irradiation) as the dislodged atoms diffuse out (Egerton, 1980).

Coating both sides of a TEM specimen with carbon (or a metal) has been shown to have a protective effect, reducing

Table 3

Characteristic dose for the removal of specified elements from organic specimens irradiated with 80 keV electrons, determined by EELS (Egerton et al., 1987)

Material	Element	$D_e$ (C/cm <sup>2</sup> ) at 300 K	$D_e$ (C/cm <sup>2</sup> ) at 100 K
Collodion	N	0.002	0.25
	O	0.006	0.5
	C	0.06	0.3
Formvar	O	0.03	~1
PMMA	O	0.06	0.5
	C	0.5	0.8
Polycarbonate	O	0.5	>5
Cl <sub>16</sub> Cu Pc	Cl	~3	~10

mass loss (Table 4). A possible explanation is that the coating acts as a diffusion barrier, reducing the escape rate for light gaseous elements. Researchers studying the composition of interfaces (using a highly focused electron probe) have been known to pre-irradiate the area of interest in an older TEM, producing a thin contamination layer on each surface which inhibits the loss of light elements.

More surprisingly, surface coating is also found to reduce the loss of crystallinity (see Table 4). One proposed explanation is that return to the original molecular state (healing of the broken bond) is more likely if the escape of volatile elements is prevented (Fryer and Holland, 1983). Increasing the thickness of a specimen should also reduce the out-diffusion rate and indeed the dose required to destroy crystallinity has been found to increase with increasing thickness (Fryer, 1984).

For inorganic materials, Strane et al. (1988) have suggested that coating reduces the rate of desorption-induced electronic transitions (DIET). Coating might also reduce beam-induced temperature rise or electrostatic charging (Salih and Cosslett, 1974), besides acting as a sputtering barrier (as discussed earlier).

Table 4

Effect of surface coating on radiation sensitivity of TEM specimens; Pc denotes phthalocyanine. Specimen thickness was in the range 7–50 nm, coating thickness in the range 5–15 nm

Measurement method	Specimen	Coating	Protection factor
EELS (O-loss)	collodion	C	1.7
EELS (Cl-loss)	Cl <sub>16</sub> Cu Pc	C	~4
EELS (F-loss)	LiF	C	1.5
	CaF <sub>2</sub>	C	5.7
Electron diffraction	Coronene	Al	3
		Au	5
Electron diffraction	Perylene	C	3.0
	Pc	C	2.7
	Cl <sub>16</sub> Cu Pc	C	6.1
	Br <sub>16</sub> Cu Pc	C	6.0

Data from Salih and Cosslett (1974); Fryer and Holland (1983, 1984); Egerton et al. (1987).

## 8. Hydrocarbon contamination

The inverse of mass loss is mass gain, and such an effect occurs when hydrocarbon molecules on the surface of a TEM or SEM specimen are polymerized by the incoming (or outgoing) electrons. This polymer has a low vapour pressure and low surface mobility, so it increases in thickness as the irradiation proceeds.

Beam-induced contamination was a severe problem in the early days of electron microscopy. Since then, the vacuum in the TEM and SEM has steadily improved, both in terms of pressure (at the specimen) and hydrocarbon content (gaseous hydrocarbons arising from pump oils, vacuum grease, O-ring seals etc.). As a result, the problem of specimen contamination has been greatly reduced; yet not eliminated since the specimen itself can act as a local source of hydrocarbons, acquired during the specimen preparation procedure or during storage or transfer through the normal air. Techniques which are used to combat this problem include the following.

1. Heat the specimen with an electric lamp in air (or in the microscope airlock) in order to desorb hydrocarbons from its surfaces. Irradiation by a small ultraviolet lamp is also said to be effective and might be preferable for heat-sensitive specimens.
2. Expose the specimen to energetic ions (which sputter away the surface layer) in a plasma cleaner or in the microscope (Isabell et al., 1999).
3. Flood the surrounding area with electrons, by defocussing the illumination and removing the condenser aperture (in TEM) or by scanning at lower magnification (in SEM) in order to fix (polymerize) surface hydrocarbons and prevent them diffusing towards a focused probe.
4. Heat the specimen to about 300 °C in the TEM, in order to desorb hydrocarbons from its surface and maintain a low hydrocarbon concentration *during* viewing.
5. Cool the specimen during observation and thereby reduce the mobility of surface hydrocarbons (Wall, 1980). If water vapour is present in the microscope vacuum, it may condense on the specimen and ‘burn off’ (oxidise) hydrocarbons within the illuminated area (Hren, 1979) but this situation is harmful to organic specimens since the specimen itself can be eroded.

It is known that the diffusion of hydrocarbons along the specimen *surface* provides the source of most hydrocarbon contamination because, for a beam which focused to a diameter  $\approx 1 \mu\text{m}$ , the contamination occurs as a ring (Hren, 1979). Hydrocarbons already adsorbed on the specimen diffuse along its surface towards the edge of the irradiated area and are immobilized there.

For smaller electron-beam diameters, a contamination peak is formed rather than a ring and this effect can be

utilized as a form of lithography, as proposed long ago by Broers (1964). Because the hydrocarbon polymer has reasonable resistance to etching by chemical solutions or sputtering ions, a dot-array contamination pattern can be used to fabricate an array of magnetic dots with data storage applications; see Fig. 7a. Alternatively, the contamination line formed by a linear electron-beam scan can be used to produce a nano-wire with interesting electrical properties, as in Fig. 7b. In this case, the line-edge roughness (LER) is of importance and the measured values ( $\text{LER} < 1 \text{ nm}$ ,  $3\sigma$ -value) compare favourably with those achievable by e-beam lithography with ultra-thin polymer resists.

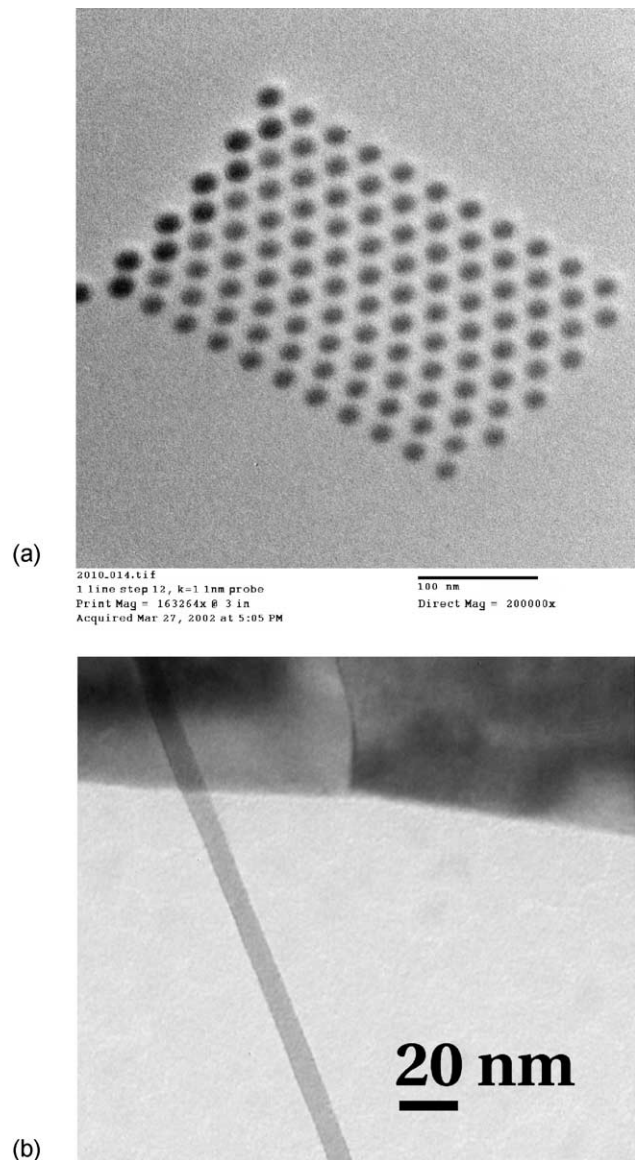


Fig. 7. (a) Array of contamination dots written on a silicon nitride membrane by an electron probe in a 200 kV TEM. (b) 7 nm-wide bismuth line with low line-edge roughness ( $\text{LER} < 1 \text{ nm}$ ), produced by contamination lithography.

## 9. Energy threshold effects

A common assumption in radiation-damage studies is that the extent of the damage depends on the amount of energy deposited in the sample by ionizing radiation (charged particles or X-rays). This postulate is implicit in the units (Gray, rad or  $G$ -value) commonly employed in radiation dosimetry (Cember, 1992; Reimer, 1989). It would imply (for example) that an electron which undergoes an inelastic collision with 300 eV energy loss produces 10 times as much damage as an electron which suffers a 30 eV collision.

In fact, there are reasons for questioning this assumption. 300 eV exceeds the binding energy ( $E_i \approx 285$  eV) of a carbon K-shell electron, so a 300 eV-loss event can cause K-shell ionization, followed by de-excitation which (in light elements) involves mainly the emission of Auger electrons. The Auger process leaves the C atom with a double negative charge which would likely damage the stable ring structure of aromatic compounds, whereas lower-energy (valence-electron) excitation might not cause such damage.

After measuring electron-beam damage in nucleic acids, Isaacson (1975) obtained a damage cross-section comparable to the K-shell ionization cross-section, leading him to suggest that only K-shell ionizations cause damage in aromatic molecules. This would lead to a threshold effect: if the incident electron energy  $E_0$  is reduced to below  $E_i$ , there should be a substantial reduction in the amount of damage to aromatic compounds.

This idea received experimental support from workers at the Cavendish laboratory (Howie et al., 1985) who irradiated  $p$ -terphenyl with electrons (of different energy  $E_0$  and with various doses) in an SEM, then determined the critical dose  $D_c$  for loss of crystallinity by observing the damaged area in a 100 keV TEM. Their damage cross-section ( $\sigma_d = e/D_c$ ) fell to unmeasurably low values as  $E_0$  was reduced below about 1 keV. The discrepancy between this threshold energy and the carbon-K ionization energy was ascribed to the competing influence of valence-electron scattering. Subsequent work on other aromatics (coronene, perylene) produced similar results (Howie et al., 1987), whereas the aliphatic compound L-valine showed no abrupt threshold—just a more gradual fall in damage cross-section below 1 keV in accordance with the lower energy deposition at low  $E_0$ . Further experiments at Arizona State University (Stevens et al., 2000) provided similar conclusions.

One problem associated with the above experimental procedure is that the electron penetration depth becomes very small at low  $E_0$ . Taking the electron range as (50 nm)  $E_0(\text{keV})^{1.35}$  for carbon (Bongeler et al., 1992) gives  $R = 50$  nm at 1 keV and  $R = 20$  nm at 500 eV. Unless the sample is thinner than the electron range, low- $E_0$  irradiation will leave an undamaged layer below the beam-entrance surface of the specimen, giving a diffraction pattern when the specimen is re-examined using high-energy electrons in

the TEM and leading to the illusion of no damage at low  $E_0$  ( $D_c \sim \infty$ ,  $\sigma_d \approx 0$ ). The Cavendish workers tried to avoid this situation by using (in their later experiments) very thin specimens, irradiated from both sides. The ASU group conducted additional experiments in which a diffraction pattern was observed at the same energy as used for the irradiation. Their observation of transmission diffraction at  $E_0 < 1000$  eV showed that some regions of the specimen were very thin and, assuming thicker regions made no contribution to the diffraction pattern, the presence of an energy threshold was apparently confirmed.

In fact, it is very difficult to make uniform-thickness samples of molecular solids such as coronene. When grown either from solution or by vacuum sublimation, a specimen consists of partially-connected crystallites separated by holes. Three-dimensional growth leads to the existence of thicker regions, even when the average thickness is below the electron range, while the statistical nature of electron scattering suggests the possibility of some contribution from underlying undamaged regions. We therefore believe that the interpretation of electron-diffraction measurements is not straightforward (Li, 2003).

As an alternative measure of radiation damage, we have made use of the fact that aromatic compounds are efficient light emitters and provide a cathodoluminescence (CL) signal in the SEM. As shown in Fig. 8, the CL yield varies with incident energy  $E_0$  in a similar way to the (calculated) energy deposition in the sample, as would be expected if the light emission is an end-result of valence-electron excitation. More significantly, we find that the CL signal decays exponentially (with characteristic dose  $D_c$ ) during irradiation, even when the incident energy is very low (landing energies below 1 keV can be achieved by applying

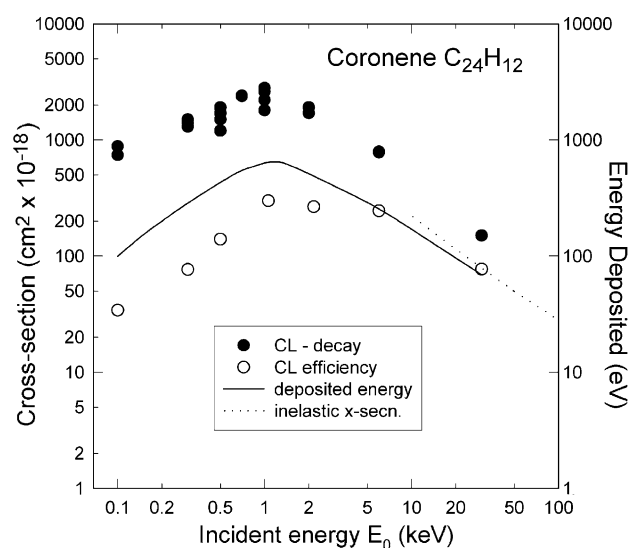


Fig. 8. Energy deposition (solid curve), CL signal normalized to the incident-beam current (open circles) and damage cross-section (solid circles) derived from time decay of the CL signal for a thin film of coronene. The dashed line shows a calculated total-inelastic scattering cross-section per molecule.

a negative bias to the specimen stage). In fact, our measured damage cross-section for CL decay ( $e/D_e$ ) also varies with  $E_0$  in proportion to the amount of energy deposition (Fig. 8). This finding indicates that valence-electron excitations are effective in producing some form of damage that results in decay of the CL signal.

Above  $E_0 = 1$  keV, the CL-decay cross-section is about 30 times larger than the damage cross-section obtained from diffraction measurements on coronene at the same energy. It is quite close to the estimated total-inelastic cross-section per coronene molecule, suggesting that (on average) each molecule emits only one photon before light emission is suppressed.

Since there is less complication from valence-electron excitation, the existence of a K-shell threshold effect could be examined with greater precision by using X-rays to create the damage and examine the effects. Employing a synchrotron source, the damage rate could be measured just above and just below 285 eV (the carbon-K threshold), making allowance for the different amount of energy absorption in these two cases.

## 10. Dependence of damage on dose rate and beam diameter

As remarked earlier, electron-beam hole drilling in metal oxides is observed to occur only above a threshold current density (e.g.  $5 \times 10^4$  V/cm), indicating that the irradiation damage depends on dose rate as well as accumulated dose. In the case of organic materials, some measurements have indicated that the current density  $J$  (the dose rate) does *not* affect the characteristic dose (Egerton et al., 1987) but these measurements were performed at low current densities ( $\ll 1$  A/cm<sup>2</sup>). Using higher current densities (1.6–16 A/cm<sup>2</sup>), Fryer (1987) found that lattice images of hydrocarbons could be recorded rapidly (in 10–100 ms) in the TEM, using a radiation dose equal to or exceeding that which would destroy the crystallinity at lower current densities.

Improved lattice images were also reported by Downing and Glaeser (1986) as a consequence of reducing the incident-beam diameter from 3  $\mu$ m to 1–2 nm. However, this improvement was attributed to a reduction of the amount of radiation-induced mechanical warping during the electron exposure.

Measurements at high dose rate and small probe diameter were reported by Varlot et al. (1997), using EELS to monitor reduction of the 7 eV  $\pi$ -resonance peak of PET (indicating destruction of the aromatic ring structure). Using a thermionic-source TEM, their characteristic dose was  $D_e = 0.1$  C/cm<sup>2</sup> for a 100 nm probe (containing 10 pA,  $J = 0.1$  A/cm<sup>2</sup>) whereas using a field-emission TEM, they measured  $D_e \approx 1000$  C/cm<sup>2</sup> for a 0.7 nm-diameter probe (250 pA,  $J = 5 \times 10^4$  A/cm<sup>2</sup>). This higher value of  $D_e$  cannot be explained in terms of

enhanced degradation due to beam heating (Payne and Beamson, 1993) since both the current and the current density were higher in the highly-focussed probe. The temperature rise should have been higher in that situation, resulting in a lower value of  $D_e$ .

Similar EELS measurements of  $\pi$ -peak fading were made on polyethylene by Siangchaew and Libera (2000) and they also yielded a substantial increase (up to a factor of 60) in the characteristic dose for the case of a small (< 100 nm) probe diameter. The proposed explanation was that a large part of the damage (to the aromatic ring structure) arises from fast secondary electrons (FSE's) whose energy is above 50 eV. FSE's are emitted almost perpendicular to the incident beam and some travel relatively large distances from their point of origin. In the case of a small probe, FSE energy is deposited *outside* the probe area, giving rise to 'collateral' damage which is not monitored by the transmitted (energy-loss) electrons. In support of this idea, Siangchaew and Libera performed digital linescans, varying the distance ( $s$ ) between pixels from 5 to 80 nm. At  $s = 80$  nm, every pixel produced the same  $\pi$ -peak intensity (for the same electron dose) whereas at  $s = 5$  nm the  $\pi$ -peak intensity was reduced (except at the first pixel) indicating that as the probe sampled previously-damaged material.

The main difficulty with the FSE explanation is that there are not enough high-energy secondaries to give a substantial enhancement factor for small probes. Consideration of the number, energy and range of the FSE's suggests that 75% of the FSE energy is deposited within 2 nm of the incident probe (Egerton and Malac, 2004). Instead, collateral damage might be caused by *slow* secondaries, for which the inelastic mean free path can exceed 2 nm in some materials if their starting energy is less than 10 eV (Seah and Dench, 1979; Cartier et al., 1997; Bass and Sanche, 1998). In insulators, the inelastic mean free path could be as long as 1  $\mu$ m (limited only by phonon processes) if the electron energy lies within the forbidden gap (Spence, 1997), although it is not clear whether these low-velocity electrons can cause damage in an organic material.

Clearly, the radiation damage produced by a small electron probe represents an important problem requiring further investigation, including measurements in which any specimen drift is carefully monitored and where the current-density distribution of the probe is measured out to a radius of at least 50 nm.

## Acknowledgements

We thank Profs A. Howie, J.C.H. Spence, M. Libera and D.C. Joy for helpful discussions and NSERC for financial support.

## References

- Bass, A.D., Sanche, L., 1998. Absolute and effective cross-sections for low-energy electron-scattering processes within condensed matter. *Radiat. Environ. Biophys.* 37, 243–257.
- Broers, A.N., 1964. Micromachining by sputtering through a mask of contamination laid down by an electron beam. In: Bakish, R., (Ed.), *Proceedings of the 1st International Conference on Electron and Ion Beam Science and Technology*, Wiley, New York, pp. 191–204.
- Broers, A.N., 1988. Resolution limits for electron-beam lithography. *IBM J. Res. Dev.* 32, 502–513.
- Cartier, E., Pfluger, P., Pireaux, J.-J., Rei Vilar, M., 1997. Mean-free paths and scattering processes for 0.1–4500 eV electrons in saturated hydrocarbon films. *Appl. Phys. A* 44, 43–53.
- Cazaux, J., 1995. Correlations between ionization radiation damage and charging effects in transmission electron microscopy. *Ultramicroscopy* 60, 411–425.
- Cember, H., 1992. *Introduction to Health Physics*, second ed, McGraw-Hill, New York.
- Cherns, D., Minter, F.J., Nelson, R.S., 1976. Sputtering in the high voltage electron microscope. *Nuclear Instr. Meth* 132, 369–376.
- Cherns, D., Finnis, M.W., Matthews, M.D., 1977. Sputtering of gold foils in a high voltage electron microscope: a comparison of theory and experiment. *Phil. Mag.* 35, 693–714.
- Clark, W.R.K., Chapman, J.N., Macleod, A.M., Ferrier, R.P., 1980. Radiation damage mechanism in copper phthalocyanine and its chlorinated derivatives. *Ultramicroscopy* 5, 195–208.
- Crozier, P.A., McCartney, M.R., Smith, D.J., 1990. Observation of exit surface sputtering in TiO<sub>2</sub> using biased secondary electron imaging. *Ultramicroscopy* 237, 232–240.
- Curtis, G.H., Ferrier, R.P., 1969. The electric charging of electron-microscope images. *J. Phys. D* 2, 1035–1040.
- Devenish, R.W., Eaglesham, Maher, D.M., Humphreys, C.J., 1989. Nanolithography using field emission and conventional thermionic electron sources. *Ultramicroscopy* 28, 324–329.
- Downing, K.H., Glaeser, R.M., 1986. Improvement in high resolution image quality of radiation-sensitive specimens achieved with reduced spot size of the electron beam. *Ultramicroscopy* 20, 269.
- Egerton, R.F., 1980. Chemical measurements of radiation damage in organic samples at and below room temperature. *Ultramicroscopy* 5, 521–523.
- Egerton, R.F., Malac, M., 2004. The lateral range and energy deposition of fast secondary electrons. submitted for publication.
- Egerton, R.F., Crozier, P.A., Rice, P., 1987. Electron energy-loss spectroscopy and chemical change. *Ultramicroscopy* 23, 305–312.
- Fryer, J.R., Holland, F., 1983. The reduction of radiation damage in the electron microscope. *Ultramicroscopy* 11, 67–70.
- Fryer, J.R., 1984. Radiation damage in organic crystalline films. *Ultramicroscopy* 14, 227–236.
- Fryer, J.R., Holland, F., 1984. High resolution electron microscopy of molecular crystals. III. Radiation processes at room temperature. *Proc. R. Soc. (London)* A393, 353–369.
- Fryer, F.R., 1987. The effect of dose rate on imaging aromatic organic crystals. *Ultramicroscopy* 23, 321–328.
- Henderson, R., Glaeser, R.M., 1985. Quantitative analysis of image contrast in electron micrographs of beam-sensitive crystals. *Ultramicroscopy* 16, 139–150.
- Hobbs, L.W., 1987. Radiation effects in analysis by TEM. In: Hren, J.J., Goldstein, J.I., Joy, D.C. (Eds.), *Introduction to Analytical Electron Microscopy*, Plenum Press, New York, pp. 399–445.
- Hobbs, L.W., 1990. Murphy's law and the uncertainty of electron probes. *Scanning Microscopy Supplement* 4, 171–183.
- Howie, A., Rocca, F.J., Valdre, U., 1985. Electron beam ionization damage processes in p-terphenyl. *Phil. Mag.* B52, 751–757.
- Howie, A., Mohd Muhid, M.N., Rocca, F.J., Valdre, U., 1987. Beam damage in organic crystals. *Inst. Phys. Conf. Ser. No. 90(Proc. EMAG 87)*, 155–158.
- Hren, J.J., 1979. Barriers to AEM: contamination and etching, *Introduction to Analytical Electron Microscopy*, Plenum Press, New York, pp. 481–505.
- Humphreys, C.J., Bullough, T.J., Devenish, R.W., Maher, D.M., Turner, P.S., 1990. Electron beam nano-etching in oxides, fluorides, metals and semiconductors. *Scanning Microscopy Supplement* 4, 185–192.
- International Experimental Study Group, 1986. Cryoprotection in electron microscopy. *J. Microsc.* 141, 385–391.
- Isaacson, M., 1975. Inelastic scattering and beam damage in biological molecules. In: Siegel, B.M., Beaman, D.R. (Eds.), *Physical Aspects of Electron Microscopy and Microbeam Analysis*, Wiley, New York, Chapter 14.
- Isaacson, M.S., 1977. Specimen damage in the electron microscope, *Principles and Techniques of Electron Microscopy*, Vol. 7. Van Nostrand, New York, 1–78.
- Isabell, T.C., Fishione, P.E., O'Keefe, C.O., Guruz, M.U., Dravid, V.P., 1999. Plasma cleaning and its applications for electron microscopy. *Microsc. Microanal.* 5, 126–135.
- Joy, D.C., Joy, C.S., 1996. Low voltage scanning electron microscopy. *Micron* 27, 247–263.
- Li, P., 2003. Electron irradiation damage to organic light-emitting materials. MSc thesis, University of Alberta, Canada.
- Lupini, A.R., Krivanek, O., Dellby, N., Nellist, P.D., Pennycook, S.J., 2001. Developments in Cs-corrected STEM. *Inst. Phys. Conf. Ser. No. 168*, 31–34.
- McCartney, M.R., Crozier, P.A., Weiss, J.K., Smith, D.J., 1991. Electron-beam-induced reactions at transition metal oxide surfaces. *Vacuum* 42, 301–308.
- Medlin, D.L., Howitt, D.G., 1991. The roles of sputtering and atomic displacement in electron irradiation induced mass loss, *Microbeam Analysis—1991*, San Francisco Press, San Francisco, 271–272.
- Payne, R.S., Beamson, G., 1993. Parallel electron energy-loss spectroscopy and X-ray photoelectron spectroscopy of poly (ether ether ketone). *Polymer* 34, 1637–1644.
- Reimer, L., 1975. Review of the radiation damage problem of organic specimens in electron microscopy. In: Siegel, B.M., Beaman, D.R. (Eds.), *Physical Aspects of Electron Microscopy and Microbeam Analysis*, Wiley, New York.
- Reimer, L., 1989. *Transmission Electron Microscopy*, second ed, Springer, Berlin.
- Reimer, L., 1998. *Scanning Electron Microscopy*, second ed, Springer, Berlin.
- Reimer, L., Golla, U., Boeneger, R., Kaessens, M., Schindler, B., Senkel, R., 1992. Charging of bulk specimens, insulating layers and free-supporting films in scanning electron microscopy. *Optik* 92, 14–22.
- Salih, S.M., Cosslett, V.E., 1974. Reduction in electron irradiation damage to organic compounds by conducting coatings. *Phil. Mag.* 30, 225–228.
- Salisbury, I.G., Timsit, R.S., Berger, S.D., Humphreys, C.J., 1984. Nanometer scale electron beam lithography in inorganic materials. *Appl. Phys. Lett.* 45, 1289–1291.
- Seah, M.P., Dench, W.A., 1979. Quantitative electron spectroscopy of surfaces: a standard data base for electron inelastic mean free paths in solids. *Surface and Interface Analysis* 1, 2–11.
- Siangchaew, K., Libera, M., 2000. The influence of fast secondary electrons on the aromatic structure of polystyrene. *Phil. Mag. A* 80, 1001–1016.
- Spence, J.C.H., 1997. STEM and shadow-imaging of biomolecules at 6 eV beam energy. *Micron* 28, 101116.
- Stevens, M.R., Chen, Q., Weierstall, U., Spence, J., 2000. Transmission electron diffraction at 200 eV and damage thresholds below the carbon K edge. *Microscopy and Microanalysis* 6, 368–379.
- Strane, J., Marks, L.D., Luzzi, D.E., Buckett, M.I., Zhang, J.P., Wessels, B.W., 1988. Encapsulation, diffusion and DIET in the electron microscope. *Ultramicroscopy* 25, 253–258.
- Thomas, L.E., 1985. Light-element analysis with electrons and X-rays in a high-resolution STEM. *Ultramicroscopy* 18, 173–184.
- Varlot, K., Martin, J.M., Quet, V., Kihn, Y., 1997. Towards sun-nanometer scale EELS analysis of polymers in the TEM. *Ultramicroscopy* 68, 123–133.
- Wall, J.S., 1980. Contamination in the STEM at ultra high vacuum, *Scanning Electron Microscopy—1980*, pp. 99–106.